General Disclaimer

One or more of the Following Statements may affect this Document

- This document has been reproduced from the best copy furnished by the organizational source. It is being released in the interest of making available as much information as possible.

- This document may contain data, which exceeds the sheet parameters. It was furnished in this condition by the organizational source and is the best copy available.

- This document may contain tone-on-tone or color graphs, charts and/or pictures, which have been reproduced in black and white.

- This document is paginated as submitted by the original source.

- Portions of this document are not fully legible due to the historical nature of some of the material. However, it is the best reproduction available from the original submission.

MASTER

ERDA/NASA

ADVANCED THERMIONIC TECHNOLOGY PROGRAM

PROGRESS REPORT NO. 22

April 1977

NASA Contract NAS3-20302

ERDA Contract EY-76-C-02-3056

Prepared By

Thermo Electron Corporation

101 First Avenue

Waltham, Massachusetts 02154

I. SURFACE STUDIES

A. SURFACE THEORY

MacColl's expression* for electron reflectivity from a bare metal surface, with the incorporation of the image potential, was transformed into the following form:

$$R = \frac{\left[\frac{4i\sqrt{E}}{\alpha}\left(\sqrt{1+\frac{V_o}{E}}-1\right)U_1+\left(\sqrt{1+\frac{V_o}{E}}+1\right)U_2\right]^2}{\left[-\frac{4i\sqrt{E}}{\alpha}\left(\sqrt{1+\frac{V_o}{E}}+1\right)U_1^*+\left(\sqrt{1+\frac{V_o}{E}}-1\right)U_2^*\right]^2}$$

Where:
- E = Kinetic energy of electron in free space (eV)
- V_o = Depth of potential inside metal (eV)
- α = 3.689
- β = 0.922
- U_1 = $U(i\beta/\sqrt{E}, 1; i\alpha\sqrt{E}/V_o)$, the confluent hypergeometric function of the second kind
- U_1^* = Complex conjugate of U_1
- U_2 = $U(1+i\beta/\sqrt{E}, 1; i\alpha\sqrt{E}/V_o)$
- U_2^* = Complex conjugate of U_2

A computer subroutine was composed for generating confluent hypergeometric functions of the second kind and of complex arguments. The solution to the Schroedinger equation for the image potential problem involves such functions. The subroutine incorporates double precision determination of complex gamma and digamma functions.

* L. A. MacColl, Phys. Rev. 56, 699 (1939).

B. BASIC SURFACE EXPERIMENTS

Auger analyses were performed on samples originally studied in the Activation Chamber. The results are discussed in the pertinent sections of this report.

C. ACTIVATION CHAMBER EXPERIMENTS

Last month it was reported that the decomposition products of cesium carbonate, deposited from tungsten or molybdenum ribbons, produced much higher work function surfaces than depositions from platinum or nickel ribbons. It was suggested that this result was due to a chemical reaction of the cesium oxide with tungsten and molybdenum, thus preventing the evaporation of cesium oxide.

Auger analysis of the sample surfaces confirmed this interpretation. The deposit produced by evaporation from molybdenum contained appreciable amounts of molybdenum. Since the molybdenum ribbon was never heated above 700 C, the presence of molybdenum in the surface can be explained by the formation of volatile molybdenum oxide from the reaction of elemental molybdenum with cesium oxide. No tungsten was found in the deposit produced by heating the tungsten ribbon. However, this result is not surprising because the vapor pressure of tungsten oxide is much lower than that of molybdenum oxide.

II. PLASMA STUDIES

A. CONVERTER THEORY

A topical report which summarizes the sheath analyses has been written. The draft copy of the report is expected to be available before June.

The work on the numerical integration of the plasma equations was continued. Combining the momentum equations of electrons and ions, one obtains

$$\frac{d}{dx}\left[nk\,(T_e + T_i)\right] \simeq -\,e\left[\frac{\Gamma_e}{M_e} + \frac{\Gamma_i}{M_i}\right] \tag{1}$$

where n is the charged particle density, Γ is the charged particle current, M is the mobility, and T is the temperature. The subscripts e and i refer to electrons and ions, respectively. Using the definitions of mobilities M_e and M_i and the boundary conditions for the ions

$$\Gamma_i = 2\,\Gamma_{r_i}$$

The extrapolated distances Z can be approximated as

$$Z = \left|\frac{1}{\phi}\,\frac{d\phi}{dx}\right| \simeq \frac{2T_i}{l_i(T_i + T_e)} \tag{2}$$

$$l_i = \frac{4\sqrt{z}}{3\sigma_{ia}\,n_a}$$

l_i is the ion mean free path, n_a is the neutral particle density and σ_{ia} is the ion-neutral scattering cross section. In the last reporting period the extrapolated distances were calculated with the value of the right hand side of Equation (2) at the end points.

The computer program has been modified to use Equation (2) to locate the position of the electrodes. The computations show that the value of $2T_i/l_i\ (T_e + T_i)$ at the end points gives an accurate value of the extrapolated distance for the emitter boundary but not for the collector boundary. The ion temperature distribution is also adjusted after each iteration.

B. ENHANCED MODE CONVERSION EXPERIMENTS

1. Particle - Spaced Diodes

Room temperature capacitance measurements indicated that a minimum spacing of about 0.3 mils can be obtained between two "laser-polished" beryllium-copper mirrors with zirconia particle spacers. One of the mirrors had been electrostatically sprayed lightly with zirconia particles having a characteristic diameter of about 5 microns ($\sim$ 0.2 mils). The mirrors, as determined by Dektak measurements, were flat to within 0.1 microns (0.004 mils). No dielectric breakdown occurred for bias potentials up to 5 volts. Shorting could be brought about if a sufficiently large interelectrode pressure was applied. Since pre-shorted capacitive characteristics could be obtained when the over-pressure was relieved, it is likely that the short was produced by an edge-edge contact rather than dielectric breakdown.

The Hewlett-Packard 4815A RF Vector Impedance Meter was used successfully to measure interelectrode capacitance on particle-spaced electrodes at typical operating temperatures.

The interpretation of the measurement is based on the lump-parameter model depicted in Figure II-1. The diode is represented by the parallel elements C_P, C_L, and R_L. C_P is the lumped parasitic capacitance of the test arrangement. The interelectrode capacitance to be measured is denoted by C_L. R_L is the inverse slope of the diode current-voltage curve at the bias potential V_b. The stray lead inductance, L_S, can be made negligible (< 0.5 μH) by connecting the diode-to-bell jar feedthroughs via a coaxial cable. L_R is the inductance of the RF coil which provides ac isolation of the diode from the dc bias source V_B if the vector impedance meter test signal is at the resonant frequency. The interelectrode spacing can then be calculated (in MKS units) from the equation

$$d = \frac{A\epsilon}{\sin|\phi| / 2\pi f |Z| - C_P},$$

where A is the interelectrode area, ϕ is the measured phase angle (<O for an RC load), Z is the measured impedance, and f is the frequency (in Hz) at which the measurement is made.

This technique was used to measure the spacing of a BaO particle spaced diode having a T_E of 1216 K and a T_C of 815 K. With the diode driven in the back emission state, an impedance of 100 Ω and a phase angle of -84° were measured. These values correspond to a spacing of approximately 1.4 mils.

Spacing tests using the RCA composite (Ba, Sr, Ca,)O coating between a molybdenum emitter and a nickel collector were continued. Raising the collector temperature resulted in higher output currents. For example, at an emitter temperature of 1568 K a change of collector temperature from 1080 to 1103 K doubled the output current from

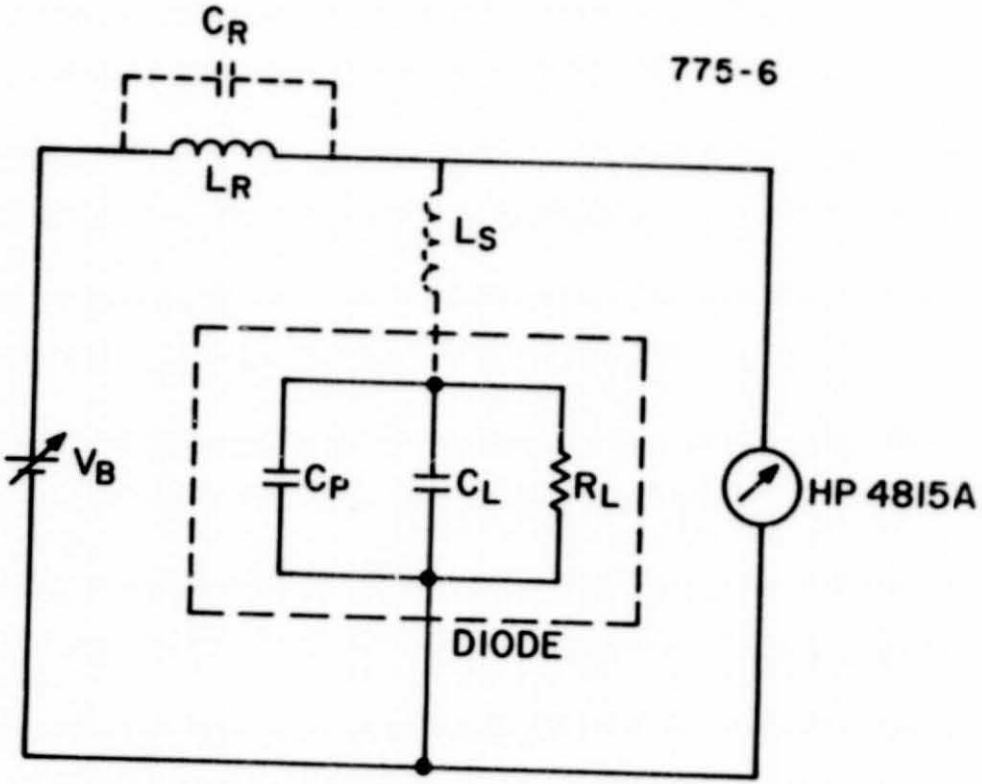

Figure II-1. Lumped Parameter Model of Test Setup for Characterization of the Particle-Spaced Diode

0.1 to 0.2 A/cm^2 for a positive 0.5 V bias across the diode. Maximum output power increased from 25 to 40 mW/cm^2. These current and power densities are based on full utilization of the 5 cm^2 surface areas of the electrodes. Dektak inspection of the electrodes after operation showed them to be crowned by over 0.5 mil. Consequently the current and power densities should be significantly increased by using uncrowned electrodes. Molybdenum mirrors polished to a surface flatness of 0.25 μm and with surface areas of 5 cm^2 have been ordered.

2. Ring Triode

Non-cesiated experiments were continued on the ring triode using the Philips Type M dispenser emitter. Manual dc I-V profiles were compared to the 60 cycle ac swept curves. Results are shown in Figure II-2. The ac curves produce substantially higher output currents, possibly due to ions created in the 4 V extremes of the sweep. Cesium was introduced into the converter. Spectral measurements made through the sapphire window in the converter by a 1/4 M monochromator confirmed the presence of both xenon and cesium in the diode. Cesium lines were seen at pressures as low as 2 x 10^{-5} torr where the converter behavior was similar to that observed without cesium.

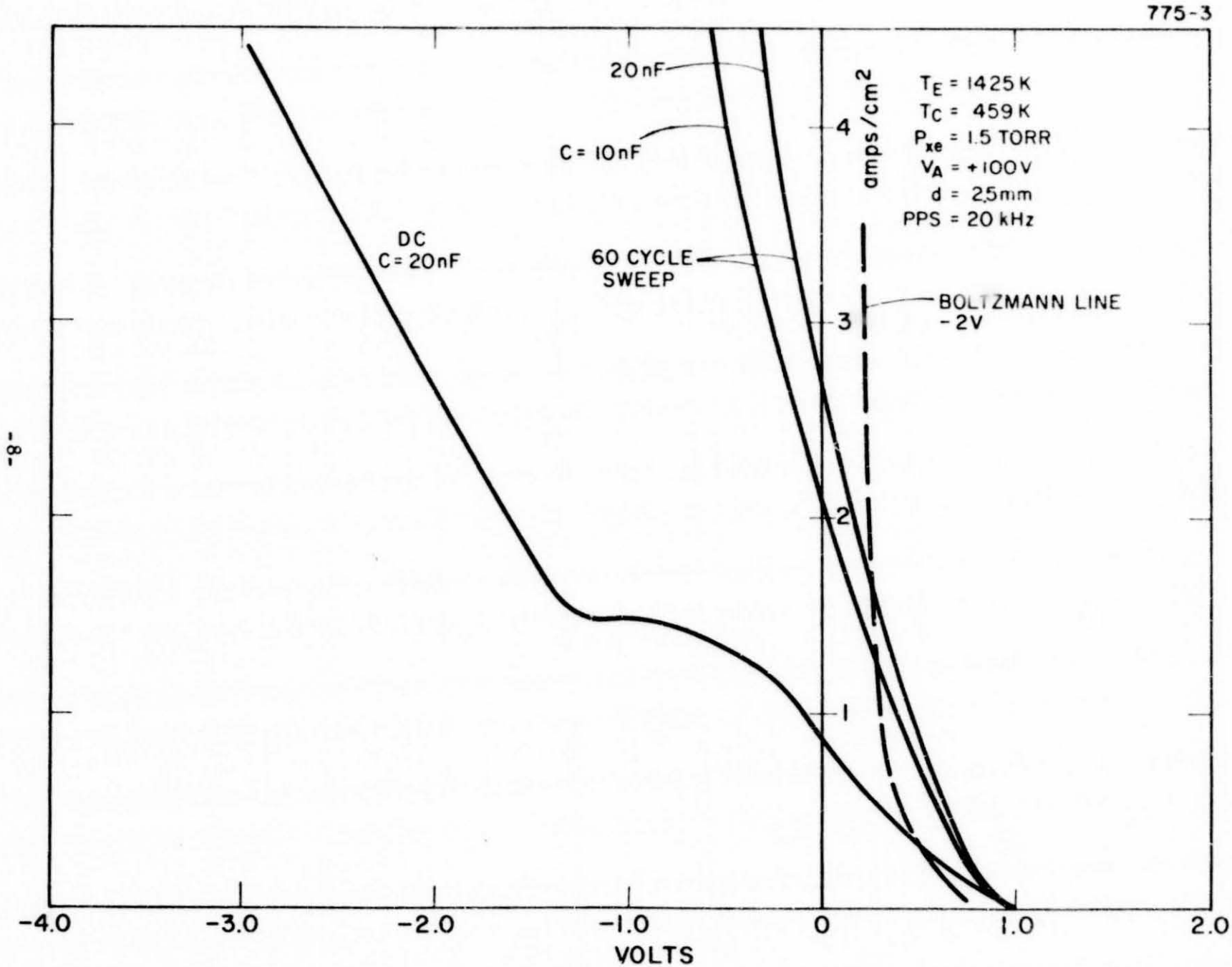

Figure II-2. DC Versus 60-Cycle AC Swept Curves

III. COMPONENT DEVELOPMENT

A. LOW TEMPERATURE CONVERSION EXPERIMENTS

1. Converter No. 17 - Barium Oxide Thin Film Diode

In an attempt to lower the bulk resistance of barium oxide when used as a collector material, a thin film barium oxide diode was constructed. The barium oxide film, approximately 800 Å thick, was evaporated onto the emitter subassembly of a standard variable spacing converter. After final welding and outgassing, the emitter will be heated to 1200 C to re-evaporate barium oxide onto the nickel collector structures to form the active surface. Tests in the Activation Chamber indicate that a barium oxide surface with a bare work function of 1.5 eV can be obtained by this evaporation method. Currently, the diode is being outgassed.

2. Powder Puff Diode

A close spaced diode was constructed with a variable spacing capability utilizing a foil membrane as a collector and a standard emitter subassembly. The standard collector structure has been modified by drilling the collector structure and welding a one mil thick tantalum foil membrane across the cavity (see Figure III-I). Pressure on the rear of the foil can be varied via tubulation to the outside of the bell jar. It is intended that the foil will flex if the emitter distorts at operating temperature. To insulate the tungsten emitter from the collector, a light coating of magnesium oxide powder was sprayed on the foil using a nitrocellulose binder. The binder will be released during outgassing of the diode.

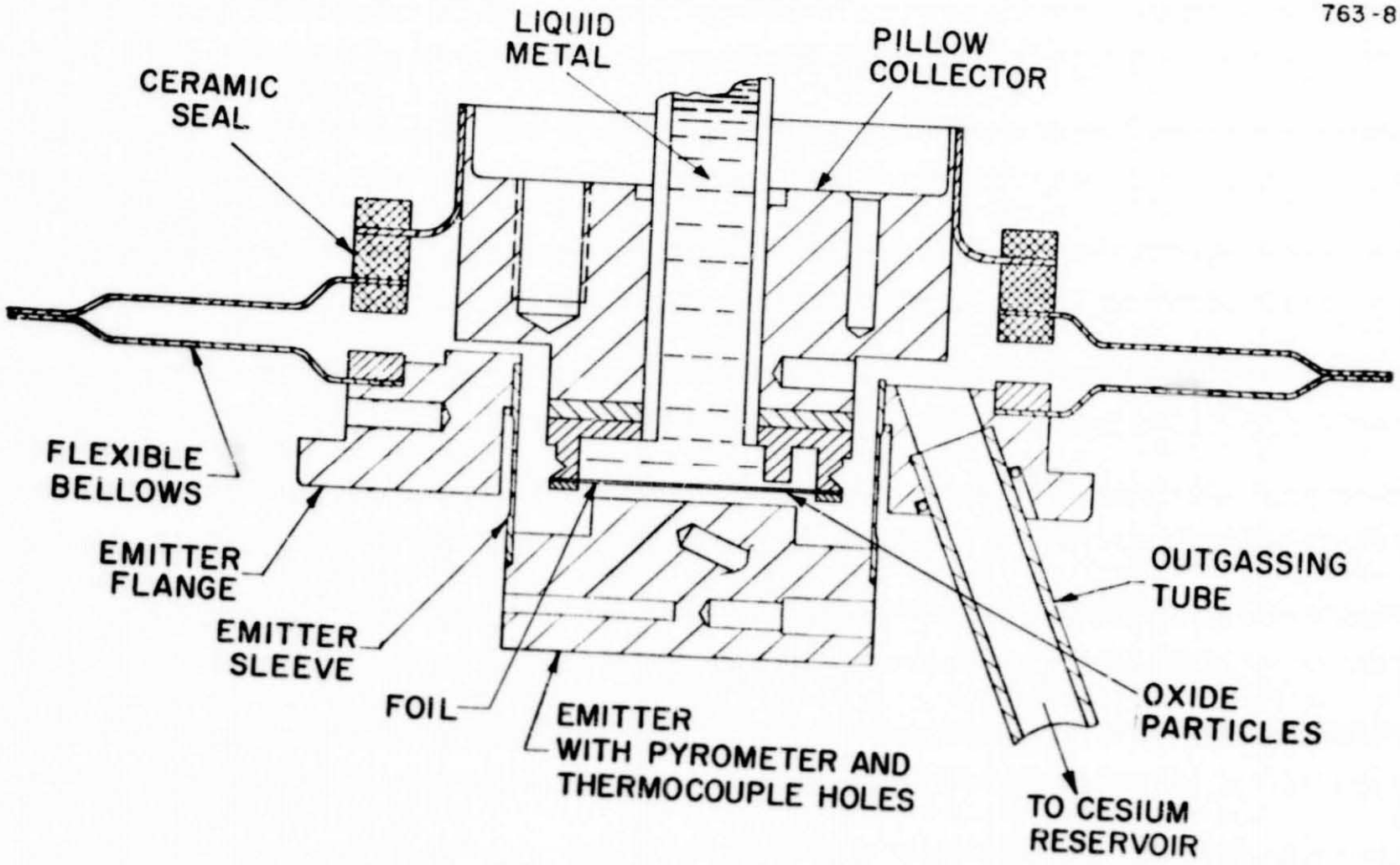

Figure III-1. Cross Section of the "Powder Puff" Diode

Room temperature vector impedance measurements over a wide range of pressures behind the foil collector gave spacings around 0.5 mil. Currently the device is being outgassed in preparation for higher temperature spacing measurements in the presence of cesium.

B. HIGH EFFICIENCY CONVERSION EXPERIMENTS

1. Converter No. 162 Tungsten Emitter - Columbium 1% Zirconium Tungsten Oxide Collector

This converter has now operated for 2200 hours at the following conditions: T_E = 1600 K, T_C = 800 K, T_R = 528 K, and d = 40 mils. The barrier index is 2.06 eV and the power output is 2.7 watts/cm^2 at 8 amp/cm^2. Life testing will continue.

2. Converter No. 165 Tungsten Emitter - Nickel Collector Heat Flux Diode

The collector heat flux was measured at collector temperatures of 650 and 850 K. The emitter temperature was held at 1600 K, the cesium reservoir at 578 K (2 torr cesium pressure) and the spacing at 20 mils. The current voltage characteristics of the converter at these conditions are shown in Figure III-2. Heat flux measurements were made using the "null" technique described in last month's report over current densities ranging from 0.5 to 4.5 amps/cm^2. The data for collector temperatures of 650 and 850 K are given in Figures III-3 and III-4. Least squares fit to these data gave slopes of 2.52 $\pm$ 0.06 watts/amp for 650 K and 2.56 $\pm$ 0.08 watts/amp for T_C = 850 K. These results are surprising since at least a 0.2 eV difference in collector work function (as indicated by the collector family in Figure III-2) was expected to be evident in the heat flux measurement. These measurements will be continued.

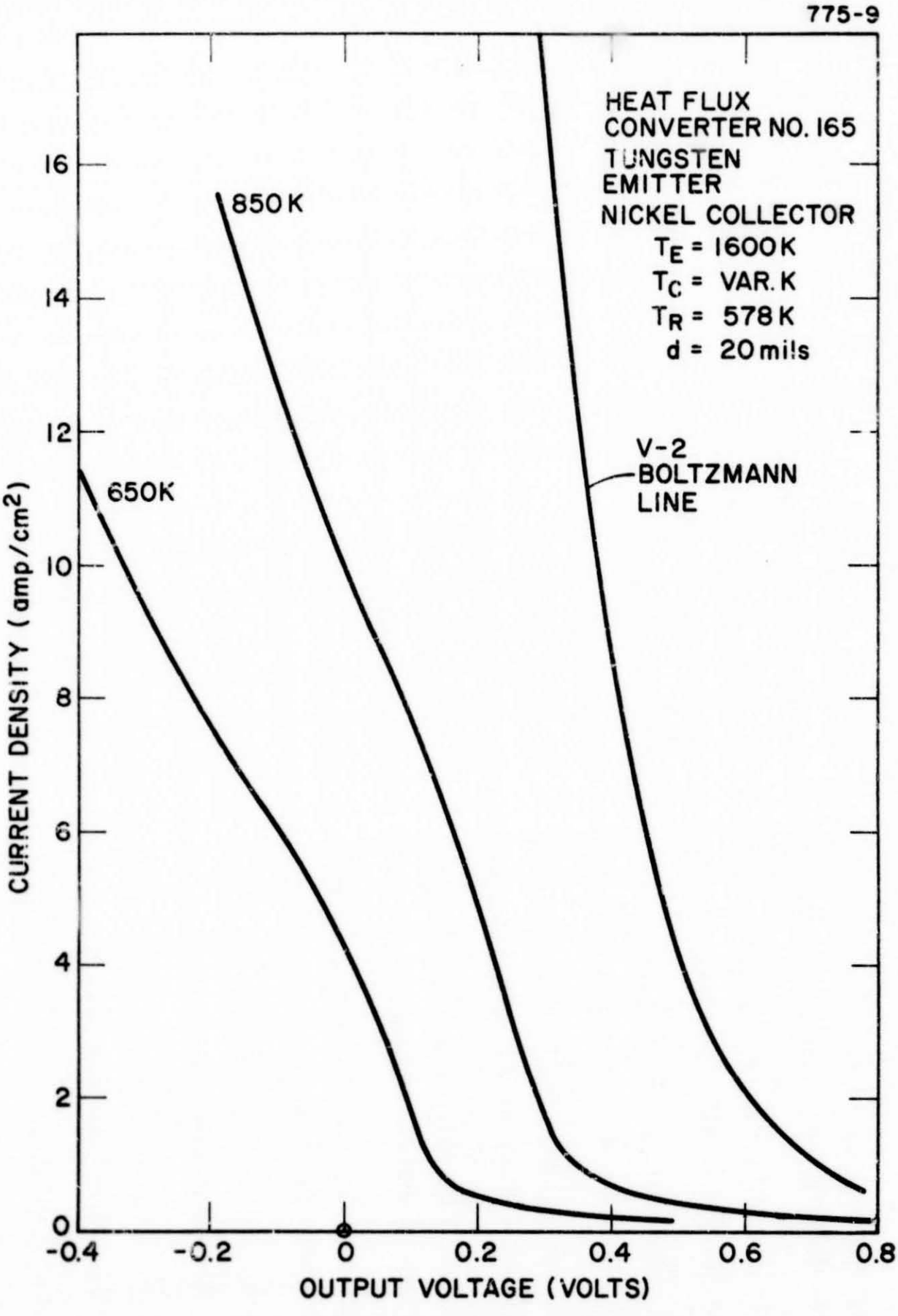

Figure III-2. Collector Family Heat Flux Diode

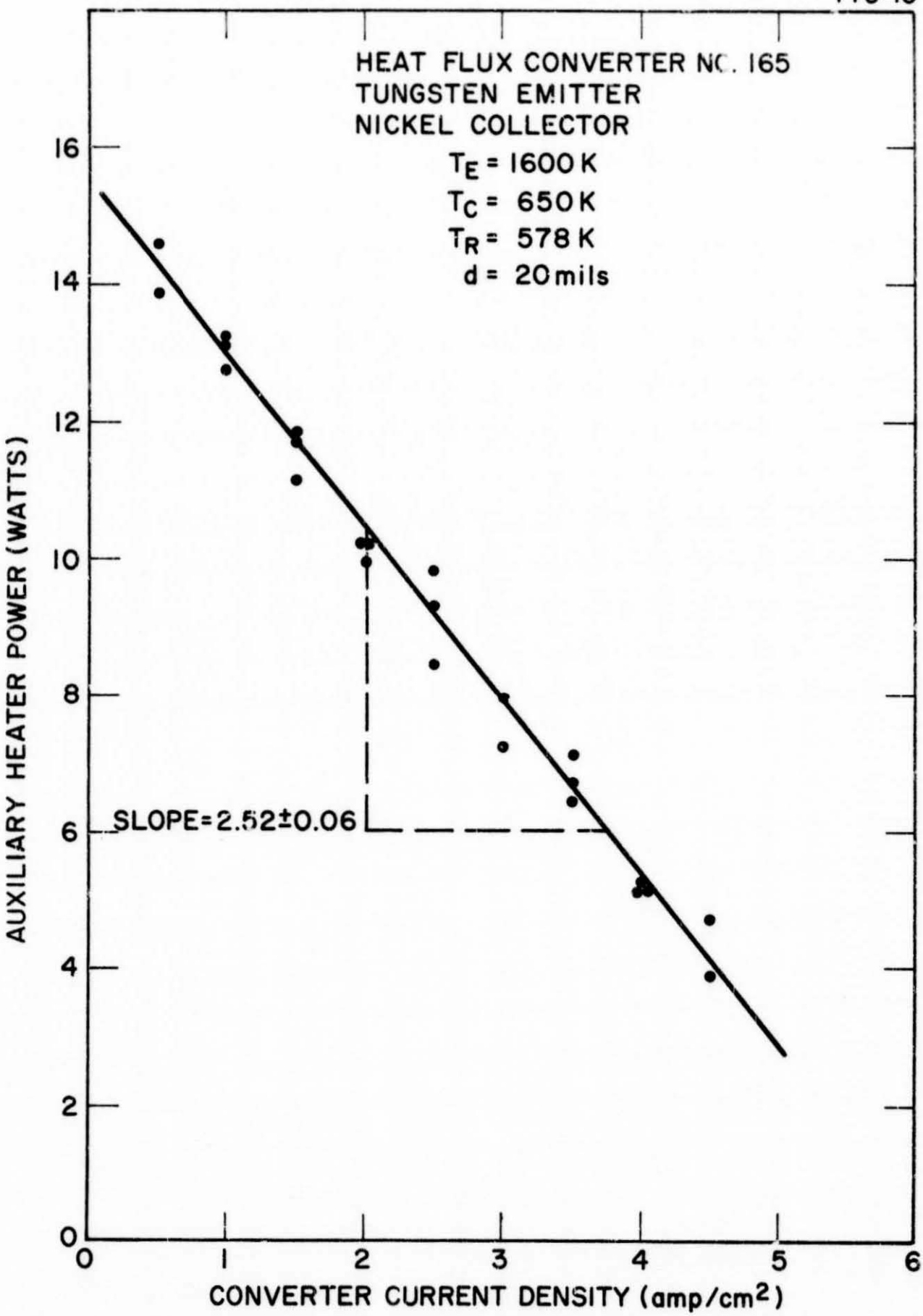

Figure III-3. Collector Heat Flux Versus Current

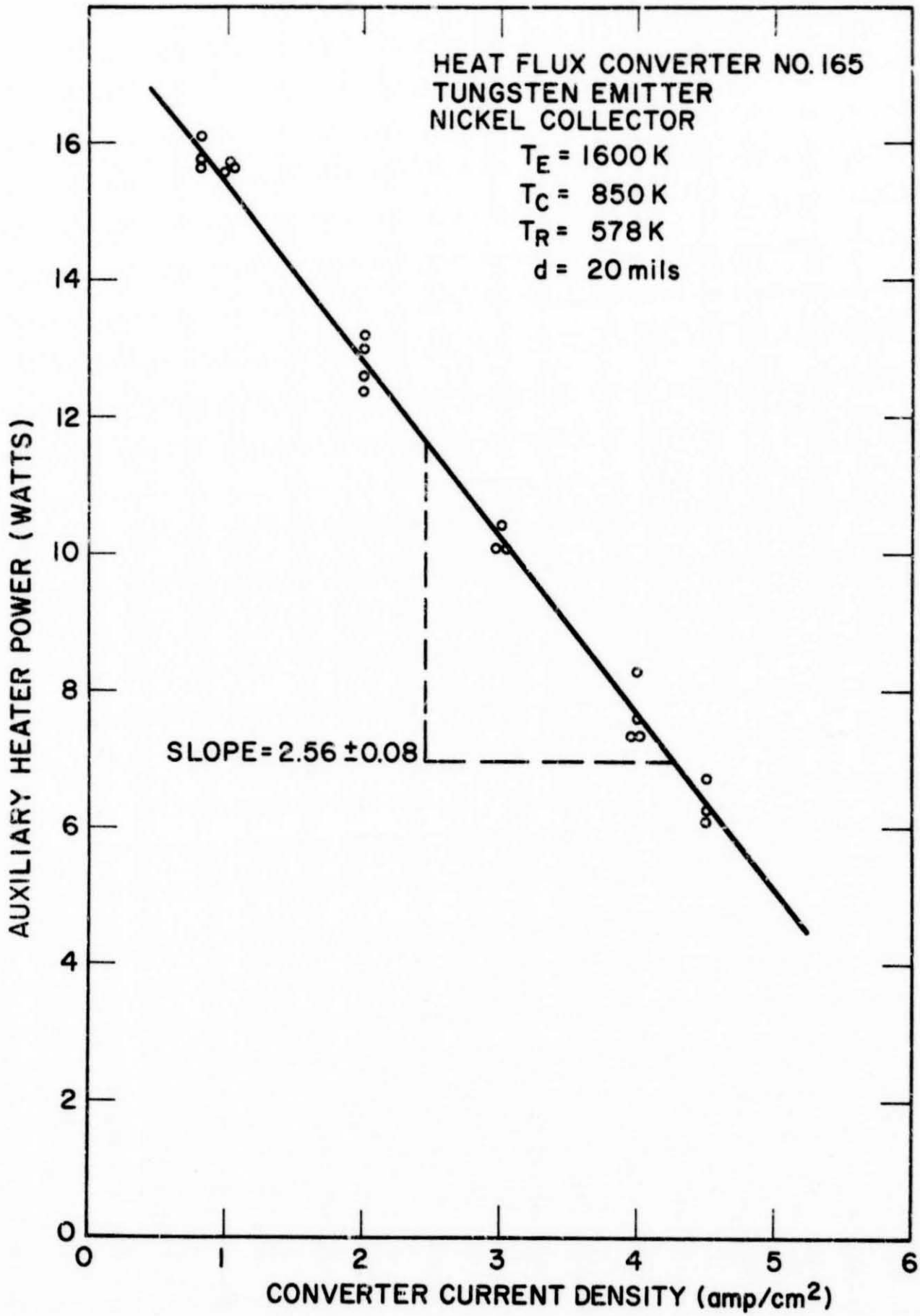

Figure III-4. Collector Heat Flux Versus Current

IV. COMPONENT DEVELOPMENT

A. HOT SHELL DEVELOPMENT

Improvement of the temperature uniformity of the graphite mandrel substrate gave, as anticipated, a corresponding improvement in silicon carbide hot shell uniformity. This uniformity was obtained by using a longer RF coil which was compressed in the region at the round end of the mandrel. Random fluctuations were noted in the RF power coupled to the graphite mandrel. Manual compensation of the fluctuations appears to have eliminated sporadic silicon deposits occasionally noticed in previously fabricated hot shells.

X-ray diffraction analyses of shells 10-C and 5-C showed them to be pure β-type silicon carbide. Cross sections of the defective braze made between the base of sample 10-C and a molybdenum adapter ring were subjected to scanning electron microprobe analysis. To within the sensitivity of the instrument, no grain boundary penetration of braze or metalizing material into the silicon carbide could be detected. Adherence of the metalization and braze materials, however, were known to be good. Fracture of the silicon during the brazing process, or immediately subsequent to it, is most likely caused by residual internal stress in the silicon carbide, a differential mismatch of thermal expansion coefficient, or a combination of both.

Simulated furnace testing continued under the following conditions: furnace gas temperature of 1300 C (2370 F), benzene combustion products flowing over the outside of hot shells, inside of shells evacuated at 10^{-7} torr. Table IV-1 presents the status of these tests as of April 29, 1977.

SIMULATED FURNACE TESTS

(April 29, 1977)

HOT SHELL	TEST HOURS	COMMENT	DATE OF TEST INITIATION
REACTION BONDED SILICON CARBIDE	11152	LEAKTIGHT THIS HOT SHELL WAS BRAZED TO A MOLYB-DENUM SLEEVE WITH NICKEL-COPPER	9 Apr. 75
KANTHAL A1	9566	LEAKTIGHT	25 Aug. 75
KANTHAL A1	9432	LEAKTIGHT	9 Sept. 75
ICONEL 671	2603	LEAKTIGHT	17 Nov. 76
CHROMIZED STAINLESS STEEL 446	2603	LEAKTIGHT	17 Nov. 76

HOT SHELL MATERIALS
TECHNOLOGY IN SUPPORT OF
ADVANCED THERMIONIC TECHNOLOGY

CONTRACT: 7070-4190-411 Mod #3

PROGRESS REPORT NO. 2

REPORTING PERIOD: 1 April through 30 April 1977

PREPARED FOR:

THERMO ELECTRON CORPORATION
101 First Avenue
Waltham, Massachusetts, 02154

Dated 9 May 1977

TRW
SYSTEMS GROUP

1.0 INTRODUCTION

This report describes the progress under contract 7070-4190-411 Mod. #3 during the period of 1 April through 30 April 1977. It is submitted as a contract deliverable summarizing the monthly technical effort.

2.0 PROGRAM OBJECTIVES AND TASKS

The objective of this program is to develop, select and evaluate candidate alloys or alloy/coating combinations as protective cover materials for thermionic devices operating as energy converters (topping cycles) in the fossil fuel combustion product environment of steam power plants.

The program has the following tasks:

- o Development of surface alloying process and evaluation of surface alloyed materials in sulfidizing-oxidizing environments of 2200-2400°F.
- o Performance of long-term and thermal cyclic tests to determine the chemical-metallurgical stability of promising mateials.
- o Investigation of fabrication process for producing hot shell shapes and fabrication of hot shell samples based on technical and economic merits as deliverables to Thermo Electron for testing.

3.0 TECHNICAL PROGRESS

During this reporting period a number of heat resistant wrought and cast Fe-Ni and Fe-Ni-Cr alloy samples were procured and several chromium surface alloying experimental runs were made.

The wrought materials are 446 S.S., 310 S.S., 309 S.S., RA26-1, INCO 690 and INCO 671. The cast materials are types HC, HA, HF, HH, HK AND HK 40.

The chemical compositions of these alloys, which will be tested either in the uncoated or surface-alloyed conditions, are tabulated in Table 1. It is planned to conduct the first hot corrosion test run at 2200°F for 100 hours in 3% excess air gas environment with the following specimens:

INCO 671
INCO 690
446 UNCOATED
446 CHROMIZED
HC UNCOATED
HC CHROMIZED
HA UNCOATED
HA CHROMIZED
HH UNCOATED
HH CHROMIZED

Current pack chromizing experiments were conducted at 1800°F, 1900°F, and 2000°F in a mixture of 30% Cr metal - 20% $CrCl_3$-50% Al_2O_3 in flowing hydrogen. Results of chromized 446, 310, 309, HC HK40, HC, HA, HF HH and HK show a deposition rate less than 0.25 mils/hour . A new chemical mixture of Cr metal -NH_4Cl-Al_2O_3 will be evaluated in the next chromizing experiments.

Concurrent with pack cementation chromizing experiments a number of 446, 309, HA and HC specimens are being chromium plated by electrodeposition. After diffusion treatment these specimens will be added to the hot corrosion test mateials list.

The hot corrosion test apparatus has been re-assembled and is being checked out. Testing is expected to resume in a week. Two separate hot corrosion test apparatus will be set up shortly for long-term and thermal cycling tests.

A. Toy
PROGRAM MANAGER

AT/dg

TABLE I

NOMINAL CHEMICAL COMPOSITIONS
OF
CANDIDATE ALLOYS

ALLOYS	Ni	Cr	Fe	Al	Co	Mo	C	Mn	S	Si	Cu	Ti	P	V	W	Cb
I N C O 671(wrought)	Bal	48					.05					.35				
I N C O 690(wrought)	60	30	9.5				.03									
446 S.S.(wrought)		25	73				.10	1.0	.015	.50			.015			
310 S.S.(wrought)	20	25	Bal				.05	1.5	.015	.50			.015			
309 S.S.(wrought)	14	23	Bal				.05	1.5	.015	.80			.015			
RA 26-1 (wrought)	0.2	26	Bal			1.0	.02	0.3		0.3		0.5	.020			
HA (cast)	0.19	9.2	Bal			.90	.18	.50	.015	1.0			.020			
HC (cast)	0.75	25	Bal			.30	.45	.50		1.0						
HK (cast)	21	25	Bal				.40	.40	.015	1.0			.020			
HK 40 Cb (cast)	22	23	Bal		.13	.10	.40	1.0	.015		.12				1.50	
HH (cast)	12.5	25	Bal			.10	.40	.50	.020	1.5			.020			
HF (cast	11	20	Bal			.40	.30	.80	.010	1.20			.030			